Int. J. Heat Mass Transfer. Vol. 24, pp. 89–97
Pergamon Press Ltd. 1981. Printed in Great Britain

0017–9310/81/0101–0089 $02.00/0

BUBBLE GROWTH RATES IN LIQUID NITROGEN, ARGON AND THEIR MIXTURES

J. R. THOME† and G. DAVEY

Cryogenics Laboratory, Department of Engineering Science, University of Oxford, England

(*Received* 14 *June* 1979 *and in revised form* 25 *March* 1980)

Abstract—The effects of liquid mixture mole fraction and vapour–liquid mole fraction difference, $y-x$, on bubble growth rates have been investigated experimentally for nitrogen–argon mixtures at 1.3 atm. The bubble growth data were obtained by processing the high speed cine films of boiling through a computerized image analysis system. Growth rates in the single components increased as the wall superheat increased and were best predicted by the Forester–Zuber growth law. In the mixtures the growth rate was dependent on the mole fraction difference, $y-x$, and was adequately modelled by the Scriven–Van Stralen mixture bubble growth term during the diffusion controlled period of growth.

NOMENCLATURE

a, bubble growth constant in $R = at^n$ [mm/s];
c_l, liquid specific heat at constant pressure [J/kgK];
D, mass diffusivity [m²/s];
$\frac{dD}{dt}$, bubble growth rate [mm/s];
$\frac{dT}{dx}$, slope of bubble line on phase diagram [K];
h_{fg}, latent heat of vaporization [J/kg];
n, bubble growth exponent in $R = at^n$;
R, equivalent bubble radius equal to $[\frac{3}{4}V]^{1/3}$ [mm];
R_i, equivalent bubble radius at time t_i [mm];
t, bubble growth time [s];
t_i, growth time relative to the designated frame of initiation of growth [s];
t_0, shift in time to the actual beginning of growth [s];
T_b, bulk liquid temperature [K];
T_w, heated wall temperature [K];
T_{sat}, saturated liquid temperature [K];
ΔT $= T_w - T_{sat}$ [K];
V, bubble volume [mm]³;
x, liquid mole fraction of the volatile component;
y, vapour mole fraction of the volatile component;
y^*, vapour mole fraction at the bubble interface.

Greek symbols

α, liquid thermal diffusivity [m²/s];
$\Delta\theta$ $= T_{sat} - T_b$, increase in temperature of liquid at bubble boundary with respect to original liquid [K];
ρ, density [kg/m³].

Subscripts

l, liquid;
m, mixture;
p, single component;
v, vapour.

INTRODUCTION

NUMEROUS reports indicate that the nucleate boiling heat transfer coefficient in binary mixtures demonstrates a minimum with respect to the pure single component coefficients in the region of the maximum mole fraction difference between the vapour and the liquid (see Thome [1] for an extensive listing of published experimental results). In order to understand why there is a reduction in the heat transfer rate and to predict the mixture heat transfer coefficient, the effect of composition on the mechanisms of boiling heat transfer have to be investigated. The parameters which could be affected are bubble growth rate, bubble departure size and frequency, bubble incipience, boiling site density, and the boiling induced turbulent convection. During the present research programme we have studied bubble growth rates and bubble departure sizes and frequencies in the isolated bubble region of the nucleate pool boiling curve. Cryogenic mixtures of liquid nitrogen and liquid argon were used in the studies. The experimentally obtained bubble growth rates are presented here.

A number of theoretical bubble growth laws have been developed for the growth of a vapour bubble in a binary mixture [2–7]. Of these, only two are in a form suited for easy use, Scriven [2] and Van Stralen [7]. Calus and Rice [8] have shown that the Scriven solution for a large superheat is equivalent to equation (27) of Van Stralen. Hence, the equation for vapour bubble growth in a binary mixture in the most convenient form of Calus and Rice is:

† Present address: Department of Mechanical Engineering, Michigan State University, E. Lansing, Michigan 48824, U.S.A.

$$R_m = \left(\frac{12}{\pi}\right)^{1/2} \frac{\Delta T \alpha^{1/2} t^{1/2}}{\left(\frac{\rho_v h_{fg}}{\rho_1 c_1}\right)\left[1 - (y^* - x)\left(\frac{\alpha}{D}\right)^{1/2}\left(\frac{c_p}{h_{fg}}\right)\left(\frac{dT}{dx}\right)\right]} \quad (1)$$

where y^* is the vapour mass fraction in the bubble corresponding to the liquid mole fraction at the liquid–vapour interface and dT/dx is the slope of the equilibrium saturation line on the phase diagram. Since $(y^* - x)$ and dT/dx are always of opposite signs, a minimum in the growth rate, dD/dt, is always predicted in the mixtures relative to the single components.

Experimentally, only two publications with extensive measurements of a large number of bubble growth cycles have been found in a literature survey. Benjamin and Westwater [9] have reported the results for the manual measurement of the initial stage of 182 bubble growth cycles for the system water–ethylene glycol at 1 atm. Yatabe and Westwater [10] extended the study to ethanol–water and ethanol–isopropanol mixtures. They fitted the growth data to an equation of the form:

$$R = at^n.$$

Minima in the dimensional growth constant and the exponent n were found in the water–glycol mixtures with respect to the single components. However, for the ethanol–water and ethanol–isopropanol systems no minima were exhibited although a concentration dependence was detected.

EXPERIMENTAL DESCRIPTION

A pool boiling cryostat with windows on opposite sides of the boiling chamber was used in conjunction with a high speed rotating prism cine camera and a light source to take cine films of bubbles growing on a heated surface. Filming speeds ranged from 1000 to 4000 frames/s. The boiling cryostat has been described previously [1, 11]. For further details of the filming setup, see Thome [1].

The cine films were analyzed by a newly developed method using a computerized image analysis system [1, 12]. Briefly, a computer program controls a film analysis machine into which the cine film is loaded. The program advances the film and records the cine film frame number, the boiling site code number, measures the magnification factor, measures the complete profile of the bubble, and then determines the volume, major diameter, and neck diameter of the bubble. The beginning and end of the waiting period and growth period of the bubble are also noted. All of these values are stored in a computer file. This method is ideal for obtaining large amounts of accurate bubble growth and departure data with relative ease.†

The boiling specimen holder is shown in Fig. 1. The boiling test surface is one end of the 20 mm dia. oxygen free-high conductivity copper rod soldered into the 0.15 mm thick stainless steel hemispherical shell. The

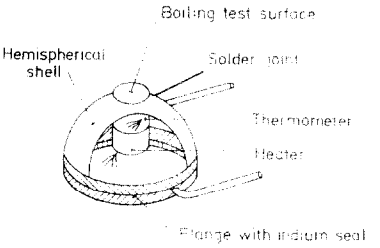

FIG. 1. Boiling specimen holder.

solder joint has been polished to retard spurious boiling. An electrical resistance heater is bolted to the opposite face of the rod to provide the heating. The wall temperature is determined with a germanium cryoresistance thermometer which is inserted 6.5 mm from the surface and then by extrapolating to the wall using the published values of thermal conductivity for OFHC copper. The saturated bulk liquid temperature is obtained with another germanium cryoresistor. The total error in wall superheat is about ± 0.10 K. The space inside the stainless steel hemispherical shell is evacuated to eliminate convection.

The boiling surface was polished before five colinear microdrilled holes spaced 2 mm apart were made to act as boiling sites, see [1] for a photograph. The microdrilled holes ranged from 21 to 52 μm in diameter with depth to diameter ratios of about 2:1. The cavities produced were cylindrical in shape. The colinear microdrilled cavities lay perpendicular to the line of site of the camera so that all would be in focus at once. A 0.925 mm dia. wire was supported directly above the cavities for focusing and to determine the magnification factor.

The pressure in the boiling chamber was measured with a pressure transducer maintained at room temperature which was connected to the chamber via a small diameter tube. Using the measured pressure (accurate to ± 0.005 bar) and the saturated bulk temperature (accurate to ± 0.1 K absolute), the liquid mole fraction of nitrogen in argon could be determined to within $\pm 1.5\%$ composition from the phase equilibrium data of Thorpe [13, 14].

The heat flux passing through the boiling surface was measured to within $\pm 1\%$.

RESULTS AND DISCUSSION

During a single 25 day cooldown to cryogenic temperature, 58 high speed cine films were taken of bubbles growing from the specially prepared boiling surface. Of the films taken, 22 were of sufficient quality to measure and 12 were compatible with the computerized measurement system. In all, 284 bubble growth cycles were measured by the computerized system. A natural boiling site was active and in focus in two instances. Bubble growth data were obtained for it.

The cine films were taken in each case when steady-state conditions resumed after the heat flux was reduced from a higher flux to the desired level. The

† This system is available for general use.

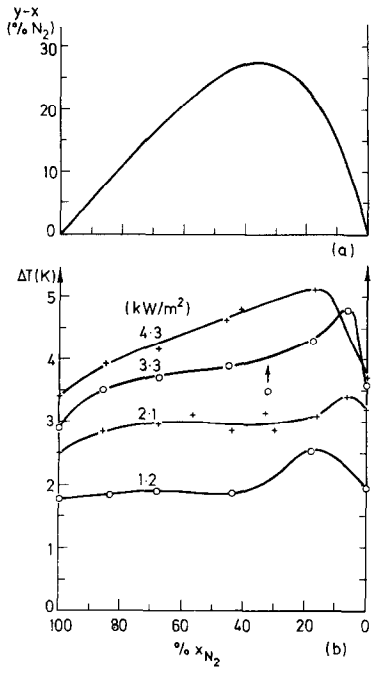

FIG. 2. (a) Vapour–liquid mole fraction difference for nitrogen—argon at 1.3 atm. (b) Wall superheat vs liquid nitrogen mole fraction in argon.

boiling curves obtained during the filming were presented in [1]. The wall superheat vs the liquid mole fraction at the four heat flux levels tested are depicted in Fig. 2 along with a plot of the vapour–liquid mole fraction difference. The wall superheats for nitrogen taken 25 days apart agreed within 0.2 K. Thus, the boiling surface was stable. The twelve cine films compatible to the computerized measurement system were primarily at the 2.1 kW m^{-2} heat flux level for the mixtures and for several levels in pure nitrogen and pure argon. For further pool boiling results, see Thome [1, 11].

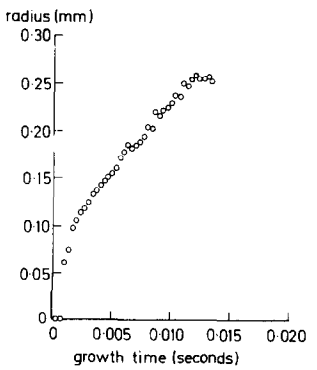

FIG. 3. Bubble growth curve of equivalent bubble radius vs growth time for a tubular bubble growing in a 68.4% nitrogen mixture ($\Delta T = 2.99$ K at $Q/A = 2.14$ kW m^{-2}).

BUBBLE SHAPES

Three bubble shapes were observed from viewing the cine films. Photographs and bubble profile traces illustrating the growth are available in [1]. At low superheats in the single components, spherical bubbles with thin necks of attachment grew from the artificial sites. At higher superheats in the single components, bubbles from the artificial and natural sites had a tubular shape, i.e. a nearly cylindrical shaped base with a hemispherical capped top. In the mixtures, no boiling sites were active at the lower superheatings. Thus, no spherical bubbles with necks were sighted. At higher superheats in the mixtures, only tubular and hemispherical bubbles occurred. The tubular bubbles grew from both the artificial and natural sites. The hemispherical bubbles actually started growth as a minor spherical segment and continued growing as a spherical segment through hemispherical shape and on to become a completed sphere at departure. These hemispherical bubbles only formed at natural sites on the polished copper surface.

In processing the cine films through the computerized system, as many as 25 consecutive bubble growth cycles were measured at a boiling site. Figure 3 shows a bubble growth cycle (equivalent bubble radius vs growth time) for a tubular bubble growing from site 4 (46 μ dia.) in a 68.4% nitrogen mixture.

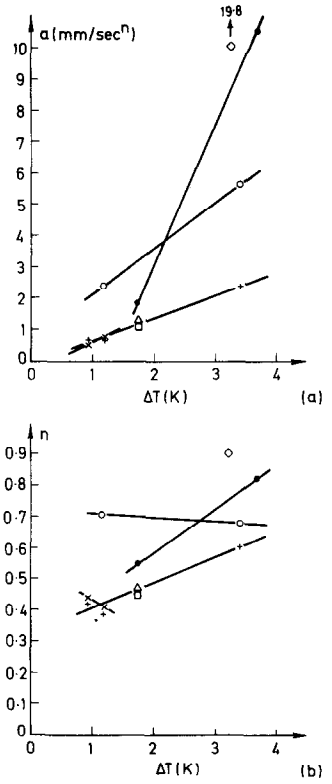

FIG. 4. Average bubble growth parameters at various boiling sites vs wall superheat. (a) Growth constant a; (b) growth exponent n. Legend: nitrogen (× site 1, 52 μm dia.; + site 4, 46 μm; ○ site 5, 21 μm); argon (△ site 1; ◇ site 2, 49 μm; ● site 3, 40 μm; □ site 4).

CURVEFITTING THE BUBBLE GROWTH DATA

The growth data was curvefitted by computer with a least squares method by minimizing the function for m data points as:

$$\text{Residual} = \sum_{i=1}^{m} [R_i - a(t_i - t_0)^n]$$

where R_i are the measured bubble radii at times t_i, t_i is the growth time relative to the computer designated frame of beginning of growth, t_0 is the shift in time from the designated start of growth to the actual beginning of growth, a is the bubble growth constant, and n is the bubble growth exponent. An iterative solution obtained the values for a, n and t_0. The results for each individual bubble growth cycle can be found in Appendix 3 of [1].

EFFECT OF SUPERHEAT ON BUBBLE GROWTH IN PURE LIQUIDS

The bubble growth parameters a and n have been studied for the pure single components, nitrogen and argon. The dependence of their growth constants and exponents on the wall superheat, ΔT, are shown in Fig. 4. Every data point for a and n is a mean value calculated from the values for each growth cycle in the sequence of growing bubbles at that particular experimental condition (see Fig. 5(a) for the number of growth cycles/sequence). The standard deviation in n and a for a particular sequence was usually about ± 15 and $\pm 30\%$, respectively. This clearly supports the conclusion of Hsu and Graham [15] that a mean bubble has to be determined from the distributions in n and a available. The growth constant increased as the wall superheat increased for each of the sites. The exponent n also increased as the wall superheat increased for boiling sites 3 and 4. Sites 1 and 5 showed slight decreases. The growth parameters for sites 1 and 4 in both argon and nitrogen demonstrated a fair agreement for bubble growth in the two liquids.

The increase in the bubble growth constant in Fig. 4(a) with increasing superheat is predicted by the theoretical bubble growth laws, such as those of Scriven [2], Plesset and Zwick [16], and Forester and Zuber [17]. All three laws predict that the growth constant, a, is linearly proportional to ΔT. While the three data points for site 4 are nearly linear, insufficient data points are available to definitely define the functional relationship of a to ΔT.

Five bubble growth laws for single component liquids have been quantitatively compared to the bubble growth constant data in Fig. 4(a). They were those of Fritz and Ende [18], Scriven for both small and large superheats [2], Plesset and Zwick [16], and Forester and Zuber [17]. Several other growth laws were not included because their growth constants are not an explicit term but two separate terms [19, 20]. The physical properties involved in the calculation of the growth constants were presented in Thome [1].

The Plesset–Zwick and Forester–Zuber growth laws gave the best agreement with the data. A comparison of the experimentally obtained growth constants, a_{exp}, to the Plesset–Zwick growth constant, a_{PZ}, and the Forester–Zuber growth constant, a_{FZ}, is given in Table 1. Boiling sites 1 and 4 showed good agreement to the theoretical growth constants with the Forester–Zuber growth law giving the better prediction. Sites 2 and 5 varied drastically from the theoretical growth models with growth exponents deviating substantially from the theoretical value of one-half.

The change in the growth exponent n with superheat needs explanation as it is not predicted theoretically. If the inertia force increases substantially as the wall superheat increases, then the bubble growth rate may be expected to pull away from the heat diffusion controlled solution of $n = 0.5$ and tend to the inertia controlled solution of $n = 1$. Thus, the increase in the growth exponent n for sites 3 and 4 as the wall superheat increased seems at first glance to be due to the 22- and 45-fold increase, respectively, in the bubble inertia force. However, the bubble inertia force for sites 1 and 5 also increased while their exponents decreased slightly. Hence, the change in n cannot satisfactorily be explained by the change in the inertia forces. Instead, the growth exponent seems to decrease as the superheat increases as long as the bubble shape remains the same. This is illustrated by the spherically shaped bubbles with thin necks forming at sites 1 and 4 for superheats of 0.93 and 1.17 K and also for the tubular shaped bubbles growing at site 5 from 1.17 to 3.4 K,

Table 1. Comparison of experimental growth constants to theoretical predictions

Nitrogen					Argon				
Site No.	ΔT [K]	a_{exp} [mm/s^n]	a_{PZ} [mm/s$^{1/2}$]	a_{FZ} [mm/s$^{1/2}$]	Site No.	ΔT [K]	a_{exp} [mm/s^n]	a_{PZ} [mm/s$^{1/2}$]	a_{FZ} [mm/s$^{1/2}$]
1	0.93	0.51	0.73	0.66	1	1.76	1.28	1.40	1.27
1	1.17	0.73	0.93	0.84	2	3.21	19.8	2.55	2.32
4	0.93	0.56	0.73	0.66	3	1.76	1.82	1.40	1.27
4	1.17	0.70	0.93	0.84	3	3.67	10.6	2.92	2.65
4	3.40	2.35	2.69	2.44	4	1.76	1.25	1.40	1.27
5	1.17	2.40	0.93	0.84					
5	3.40	5.62	2.69	2.44					

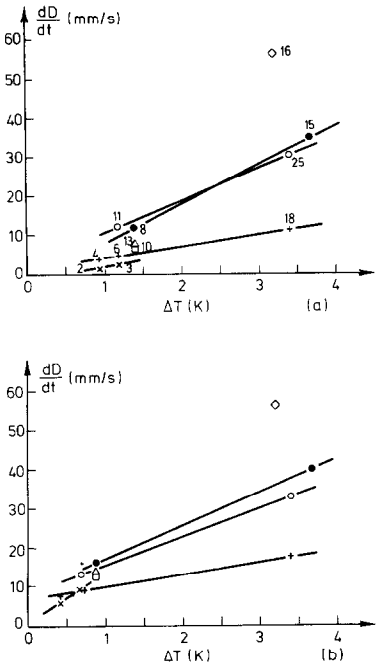

FIG. 5. Average bubble growth rate at a boiling site vs wall superheat. (a) dD/dt evaluated at times noted in text. (b) dD/dt evaluated at 0.01 s. Legend: same as for Fig. 4. (Number near data point indicates the number of sequential bubble growth cycles measured and averaged to obtain the data point.)

Fig. 4(b). Then, when the shape changes from spherical to tubular as for site 4 with ΔT going from 1.17 to 3.4 K, the exponent increases. Also for site 3 in argon, the exponent again increases when the bubble shape changes from an intermediate shape between spherical and tubular at $\Delta T = 1.76$ K to tubular at $\Delta T = 3.67$ K. Thus, the exponent seems from this limited set of data to be a function of both bubble shape and wall superheat.

The actual bubble growth rate, i.e. the rate of change in the bubble diameter with time, can be used to characterize bubble growth and avoids the dimensional problem associated with the growth constant [mm/s^n] due to varying n. It can be determined from the values of a and n at chosen times t during the growth as $dD/dt = 2ant^{n-1}$. This seems to be a better approach than non-dimensionalizing the growth constant as Benjamin and Westwater [9] have done. In order to compare the bubble growth rates as the wall superheat increases at each individual boiling site, dD/dt has been evaluated with the same value of t for the various superheats at the boiling site. In Fig. 5(a) dD/dt is plotted for five sites. The times chosen to evaluate dD/dt were near the end of the growth period of the shortest average growth time at the particular boiling site. Hence, site 1 for nitrogen was evaluated at 0.1 s which is near the average growth time of 0.103 s at $\Delta T = 1.17$ K, and less than that of 0.253 s at 0.93 K. Accordingly, for nitrogen site 4 was evaluated at 0.03 s and site 5 at 0.013 s. For argon, site 1 was evaluated at 0.03 s, site 2 at 0.01 s, site 3 at 0.02 s, and site 4 at 0.04 s. The average growth rate dD/dt at a boiling site increased with superheat in all four cases.

In Fig. 5(b), all the bubble growth rates were evaluated at 0.01 s to compare the various boiling sites at the same instant during growth. The slopes of the lines through the data differ but not drastically. Looking only at the nitrogen results, site 5 with the smallest cavity diameter (21 μ) always has a higher growth rate, dD/dt, than the larger sites, 1 (52 μ) and 4 (46 μ). This suggests that the growth rate increases as the cavity diameter decreases. However, the argon data contradict this trend. Note that the growth rates for sites 1 and 4 in nitrogen are quite comparable to those in argon.

BUBBLE GROWTH IN BINARY MIXTURES

The bubble growth parameters a and n have been obtained with a number of nitrogen–argon mixtures (see Appendix 3 of [1] for a complete listing of the parameter values). Average values of a and n have been determined for each sequence of bubble cycles, i.e. an average bubble was determined from the statistics for 5 to 24 bubbles, at a particular boiling site. The results are plotted vs % nitrogen mole fraction in Fig. 6. They were obtained at a constant heat flux level of 2.10 ± 0.06 kW m^{-2}. The films for 86 and 100% nitrogen could not be analyzed by the computerized image

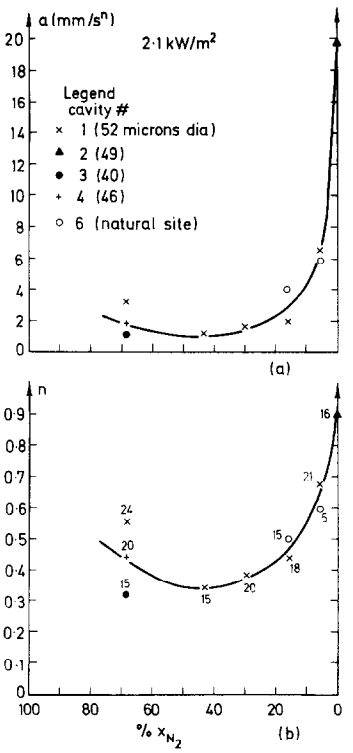

FIG. 6. Average bubble growth parameters at various boiling sites vs liquid nitrogen mole fraction % in argon. (a) Growth constant a; (b) Growth exponent n. (Number near data point indicates the number of sequential bubble growth cycles measured and averaged to obtain the data point.)

analysis method due to the close proximity of the desired bubbles to spurious bubbles growing from the solder joint being situated in nearly the same line of sight to the camera. A broad minimum in a and n at about 44% nitrogen mole fraction was found. Boiling site 1 is represented by five data points at 2.10 kW m^{-2} which would fit a curve without much scatter. The natural boiling site 6 in the polished copper surface behaved the same as the artificial sites.

The Scriven–Van Stralen bubble growth coefficients of equation (1) can be rearranged to show the effect of the mass diffusion in the mixtures relative to the single components. The Plesset and Zwick bubble growth law for a single component liquid is:

$$R_p = \left(\frac{12}{\pi}\right)^{1/2} \frac{\alpha^{1/2}\,\Delta T}{\left(\frac{\rho_v h_{fg}}{\rho_l c_l}\right)} t^{1/2} = a_{PZ} t^{1/2}. \qquad (2)$$

Thus, from equation (1) the mixture growth law can be written in terms of the Plesset and Zwick single component law as:

$$R_m = R_P \left[\frac{1}{1-(y^*-x)\left(\frac{\alpha}{D}\right)^{1/2}\left(\frac{c_l}{h_{fg}}\right)\left(\frac{dT}{dx}\right)}\right]. \qquad (3)$$

The mixture factor for nitrogen–argon at 1.3 atm has been calculated and is shown in Fig. 7. The minimum is at about 22% nitrogen mole fraction and the growth constant is reduced only about 15% compared to the massive reduction in the growth constant as shown in Fig. 6(a). However, since the experimentally measured growth exponents differ from the theoretical value of 0.5, this is not a completely satisfactory way to test the Scriven–Van Stralen equation.

The mixture bubble growth rate, dD_m/dt, can be determined from equations (2) and (3) as:

$$\frac{dD_m}{dt} = a_{PZ}\left[\frac{1}{1-(y^*-x)\left(\frac{\alpha}{D}\right)^{1/2}\left(\frac{c_l}{h_{fg}}\right)\left(\frac{dT}{dx}\right)}\right] t^{-1/2} \qquad (4)$$

or

$$\frac{dD_m}{dt} = \left[\frac{1}{1-(y^*-x)\left(\frac{\alpha}{D}\right)^{1/2}\left(\frac{c_l}{h_{fg}}\right)\left(\frac{dT}{dx}\right)}\right]\frac{dD_p}{dt}. \qquad (5)$$

The theoretical mixture growth rates can be calculated using the physical property equations for nitrogen–argon mixtures presented in Thome [1] and from the measured superheats given in Fig. 2. The range of superheats at 2.1 kW m^{-2} is 3.09 ± 0.33 K, i.e. ± 10%. Hence, the calculated growth rate dD_m/dt will only be affected by the spread in superheats by ± 10% also. The values of y^* and x at the bubble interface are assumed to be equal to the equilibrium values. The experimental mixture growth rates can be determined by $dD/dt = 2ant^{n-1}$ as was done for the single components.

To evaluate and compare the theoretical and experimental growth rates, a growth time t has to be chosen. Since the Scriven–Van Stralen equation was derived for the mass diffusion controlled stage of growth, a time should be chosen when all the bubbles are in that stage of growth. The shortest average growth time in the group at 2.1 kW m^{-2} is 0.00544 s while the longest is 0.0134 s. Hence, a choice of 0.005 s should satisfy the requirements.

Figure 8 shows the comparison between the theoretical and experimental results. The microdrilled boiling sites 1, 3 and 4 are represented quite well quantitatively. Microdrilled site 2 and natural site 6 are about double the predicted values. But, in a relative sense, the slopes obtained by connecting the mixture data points of each particular site agree well with the theoretical prediction, validating the multiplying factor in equation (5).

At the heat flux level of 2.1 kW m^{-2} in Fig. 8, only site 2 for argon (where $y-x=0$) was able to be measured using the computerized measurement system. However, since the bubble growth rate, dD/dt, is theoretically linearly dependent on ΔT, interpolated

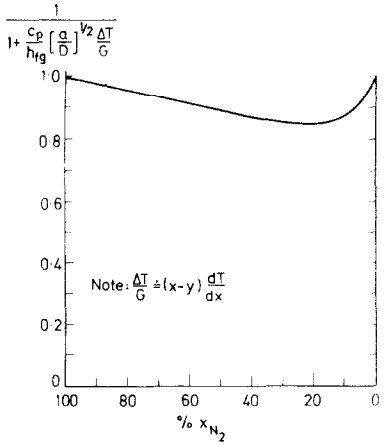

FIG. 7. Scriven–Van Stralen mixture factor for nitrogen–argon at 1.3 atm.

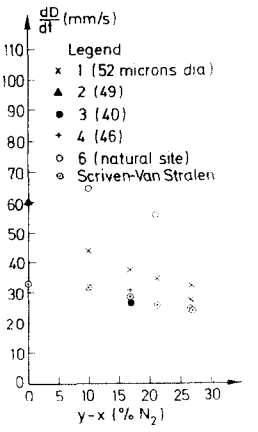

FIG. 8. Comparison of experimental bubble growth rate and Scriven–Van Stralen equation (evaluated at 0.005 s).

values of dD/dt at $\Delta T = 3.09$ K can be determined from the data on Fig. 4. The interpolated values for sites 4 and 5 in nitrogen and site 3 in argon are 21.9, 37.8, and 46.8 mm s^{-1} at $t = 0.005$ s, respectively. Consequently, the general trend in the growth rate was to increase as $y-x$ decreased to zero as the Scriven–Van Stralen theory predicted.

In order to illustrate the effect of the concentration gradient $(y-x)$ and mass diffusion on the bubble growth rate, dD/dt has been evaluated for growth times ranging from early growth up to departure. The results are shown in Fig. 9. For both artificial site 1 (Fig. 9(a)) and natural site 6 (Fig. 9(b)), the growth rate is initially higher at the more volatile mole fractions. Then at growth times of 0.002 and 0.003 s the growth rate decreases more rapidly in the more volatile mixtures. For growth times greater than 0.003 s, the growth rate is apparently being limited since the lines through the data points nearly stop rotating and become parallel. The growths do not reach this limit until about halfway through their growth periods. Since equation (5) only satisfactorily represents the data after this limit has been reached, the earlier part of growth requires further analysis.

Van Stralen's equation with the modified Jacob number for mixture bubble growth [22] is:

$$R_m = \left(\frac{12}{\pi}\right)^{1/2} Ja_m t^{1/2} \tag{6}$$

where

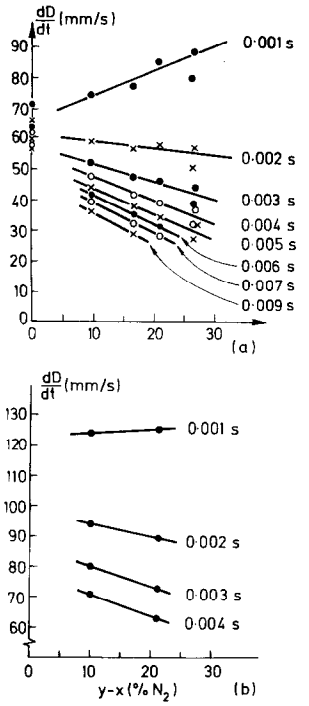

FIG. 9. Bubble growth rates as a function of growth time and vapour–liquid mole fraction difference at 2.1 kW m^{-2}; (a) site 1; (b) site 6. Site 2 with liquid argon is shown in (a) for comparison.

$$Ja_m = \frac{\rho_l c_l}{\rho_v h_{fg}} (\Delta T - \Delta\theta). \tag{7}$$

The wall superheat ΔT equals $T_w - T_{sat}$. $\Delta\theta$ represents the increase in the local saturation temperature due to the preferential evaporation of the volatile component. Van Stralen derived his equation assuming that $\Delta\theta$ was constant throughout the growth period. However, physically it is easy to surmize that $\Delta\theta$ is zero until the beginning of growth when vaporization begins. As the bubble proceeds to grow, $\Delta\theta$ increases due to preferential evaporation until the bubble growth is limited by the mass diffusion of the volatile component to the bubble interface, i.e. Van Stralen's solution. Thus, in the early stage of growth $\Delta\theta$ is a function of the growth time as well as the vapour–liquid mole fraction difference, $y-x$. This produces the rotation of the line through the data points from $t = 0.001$ to 0.003 s at which time $\Delta\theta$ has reached its maximum and the growth is controlled by mass diffusion.

CONCLUSIONS

1. The bubble growth constant and the bubble growth rate increase as the wall superheating and heat flux increase.
2. The Forester–Zuber growth law gives the best prediction of the experimental results but is only partially successful.
3. The bubble growth exponent is a function of both bubble shape and wall superheat.
4. There is a minimum in the bubble growth constant and exponent in the mixtures with respect to the single components.
5. The mixture bubble growth rate is linearly proportional to $(y-x)$, decreasing as $(y-x)$ increases.
6. The Scriven–Van Stralen mixture bubble growth term adequately represents the bubble growth rate during the mass diffusion controlled stage of growth.

Acknowledgements—The research was supported by the British Science Research Council. J. R. Thome acknowledges the receipt of a Research Grant from the Heat Transfer-Fluid Flow Service at AERE Harwell, Berkshire, England.

REFERENCES

1. J. R. Thome, Bubble growth and nucleate pool boiling in liquid nitrogen, argon, and their mixtures, D. Phil. Thesis, University of Oxford, England (1978).
2. L. E. Scriven, On the dynamics of phase growth, *Chem. Engng Sci.* **10**(1), 1–13 (1959).
3. P. J. Bruijn, On the asymptotic growth rate of vapour bubbles in superheated binary liquid mixtures, *Physicas' Grav.* **26**, 326–334 (1960).
4. L. A. Skinner and S. G. Bankhoff, Dynamics of vapour bubbles in binary liquids with spherically symmetric initial conditions, *Physics Fluids* **7**, 643–648 (1964).
5. N. Isshiki and I. Nikai, Boiling of binary mixtures, *Heat Transfer-Japan. Res.* **1**(4), 62–70 (1972).
6. H. J. Van Ouwerkerk, Hemispherical bubble growth in a binary mixture, *Chem. Engng Sci.* **27**, 1957–1967 (1972).
7. S. J. D. Van Stralen, Bubble growth rates in boiling binary mixtures, *Br. Chem. Engng* **12**(3), 390–394 (1967).
8. W. F. Calus and P. Rice, Pool boiling–binary liquid mixtures, *Chem. Engng Sci.* **27**, 1687–1697 (1972).

9. J. E. Benjamin and J. W. Westwater, Bubble growth in nucleate boiling of a binary mixture, *International Developments in Heat Transfer*, pp. 212–218. Boulder, University of Colorado (1961).
10. J. M. Yatabe and J. W. Westwater, Bubble growth rates for ethanol–water and ethanol–isopropanol mixtures, *Chem. Engng Symp. Series*, pp. 17–23 (1966).
11. J. R. Thome and W. B. Bald, Nucleate pool boiling in cryogenic binary mixtures, in *Seventh International Cryogenic Engng Conference*. London (1978).
12. G. Preston, J. R. Thome, W. B. Bald and G. Davey, The measurement of growing bubbles on a heated surface using a computerized image analysis system, *Int. J. Heat Mass Transfer* **22**, 1457–1459 (1979).
13. P. L. Thorpe, Liquid–vapour equilibrium of the system nitrogen–argon at pressures up to 10 atmospheres, *Trans. Faraday Soc.* **64**, 2273–2280 (1968).
14. P. L. Thorpe, The liquid equilibrium of the system nitrogen–argon at pressures up to 10 atmospheres, Internal Report, British Oxygen Co. Ltd., London (1966).
15. Y. Y. Hsu and R. W. Graham, *Transport Processes in Boiling and Two-Phase Systems*. Hemisphere, London (1976).
16. M. S. Plesset and S. A. Zwick, The growth of vapour bubbles in superheated liquids, *J. Appl. Phys.* **25**, 493–500 (1954).
17. H. K. Forester and N. Zuber, Growth of a vapour bubble in a superheated liquid, *J. Appl. Phys.* **25**, 474–478 (1954).
18. W. Fritz and W. Ende, Verdampfungsvorgang nach kinematographishen Aufuahmen auf Dampfblasen, *Phys. J.* **37**, 401 (1936).
19. B. B. Mikic, W. H. Rohsenow and P. Griffith, On bubble growth rates, *Int. J. Heat Mass Transfer* **13**, 657–666 (1970).
20. N. Zuber, Hydrodynamic aspects of boiling heat transfer, Ph.D. Thesis, University of California, Los Angeles (1959).
21. Lord Rayleigh, On the pressure developed in a liquid during the collapse of a spherical cavity, *Phil. Mag.* **34**, 94–98 (1917); *Scientific Papers*, Vol. 6. Cambridge University Press, Cambridge (1920).
22. S. J. D. Van Stralen, Heat transfer to boiling binary liquid mixtures, part 1, *Br. Chem. Engng* **4**(1), 8–17 (1959).

APPENDIX 1:
CHOICE OF t IN EQUATION (4)

The choice of the value of time used in evaluating equation (4) to obtain the Scriven–Van Stralen data points in Fig. 8 can be shown to be not important as long as it lies in the mass diffusion controlled stage of growth. Since the slope determined from equation (4) by varying the mole fraction for constant t is the same regardless of the time chosen, the only effect of choosing a different t is to translate the Scriven–Van Stralen points shown in Fig. 8 up or down while their relative positions or slope remain the same. The slope of the Scriven–Van Stralen points in Fig. 8 compares fairly well to the slopes in the diffusion controlled stage of growth for site 1 (Fig. 9(a)) and site 6 (Fig. 9(b)). The experimentally obtained slopes tend to be somewhat steeper. But, considering the errors involved, i.e. thermodynamic properties and experimental measurement of dD/dt, the agreement is good by engineering standards for any time t greater than 0.002 s.

CROISSANCE DE BULLES DANS L'AZOTE, L'ARGON LIQUIDES ET DANS LEUR MELANGE

Résumé—Les effets de la fraction molaire de mélange liquide et de la différence de fraction molaire entre vapeur et liquide, $y - x$, sur la croissance de bulle ont été étudiés expérimentalement pour des mélanges d'azote et d'argon à 1,3 atm. Les résultats ont été obtenus à partir de films à grande vitesse et un système digital d'analyse d'images. Les vitesses de croissance dans les composants purs augmentent lorsque la surchauffe de la paroi augments et elles sont bien décrites par la loi de Forester–Zuber. Dans le mélanges, la vitesse de croissance dépend de la différence de fraction molaire $y - x$, et elle est correctement modélisée par la description de Scriven–Van–Stralen pendant la période de croissance contrôlée par la diffusion.

WACHSTUMSGESCHWINDIGKEIT VON DAMPFBLASEN IN FLÜSSIGEM STICKSTOFF, ARGON UND DEREN GEMISCHEN

Zusammenfassung — Für Stickstoff-Argon-Gemische wird bei einem Druck von 1,3 atm der Einfluß der Differenz aus den Molanteilen der Flüßigkeit und des Dampfs auf die Wachstumsgeschwindigkeit der Dampfblasen untersucht. Um Angaben über die Blasenwachstumsgeschwindigkeit zu erhalten, wurden Hochgeschwindigkeitsfilme mit einem rechnergesteuerten Bildauswertungssystem untersucht. Bei den reinen Komponenten nahm die Wachstumsgeschwindigkeit zu, wenn die Wandübertemperatur größer wurde; dies kann am besten durch die Forester-Zuber-Wachstumsgleichung beschrieben werden. Bei den Gemischen war die Wachstumsgeschwindigkeit abhängig vom Unterschied der Molanteile. Wird das Blasenwachstum von der Diffusion beeinflußt, kann man die Wachstumsgeschwindigkeit durch die von Scriven und Van Stralen angegebene Gleichung gut wiedergeben.

СКОРОСТЬ РОСТА ПУЗЫРЬКОВ В ЖИДКОМ АЗОТЕ, АРГОНЕ И ИХ СМЕСЯХ

Аннотация — Проведено экспериментальное исследование влияния мольной концентрации жидкой смеси и разности мольных концентраций пара и жидкости, $y - x$, на скорость роста пузырьков в смесях азота с аргоном при давлении в 1,3 атм. Скорость роста пузырьков определялась путем обработки кинограмм с использованием счетно-аналитической системы. В каждом из компонентов в отдельности скорость роста увеличивается по мере возрастания перегрева стенки и лучше всего описывается соотношением Форестера–Зубера. В смесях скорость роста зависит от разности мольных концентраций $y - x$ и удовлетворительно описывается моделью Скривена–Ван Штралена в период, когда процесс определяется диффузией.